CNRS

Centre National de la Recherche Scientifique

INFN

Istituto Nazionale di Fisica Nucleare

The Noise Budget of Virgo+ with Monolithic Suspensions

VIR-0677A-09

Issue: 1.0

Date: Wednesday, 18 November 2009

AUTHORS

V.Fafone, I.Fiori, E.Genin, A.Gennai, D.Huet, M.Mantovani, P.Puppo, A.Rocchi, B.Swinkels, E.Tournefier, G.Vajente,

and

The Virgo Commissioning Team

VIRGO * A joint CNRS-INFN Project

Via E. Amaldi, I-56021 – S. Stefano a Macerata - 56021 Cascina, Italia.

Secretariat: Telephone.(39) 050 752 521 * FAX.(39) 050 752 550 * e-mail virgo@virgo.infn.it

Abstract

This document aims to describe and give a tentative projection of the noises expected to contribute to the sensitivity of the Virgo+ detector including the Monolithic Suspensions (V+MS). Individual technical noises are discussed and modeled; their projection is compared to the V+MS design curve. This comparison permits to better define the challenges of the MS detector, and to identify possibly needed noise reduction studies and investigations which are to be pursued before the MS installation.

Table of Contents

1 Introduction

Figure 1.1 shows a typical noise budget of October 2009. We have achieved a quite good understanding of the sensitivity curve of the *Virgo+* first phase (with 17W of input power and thermal compensation of input mirrors). We have succeeded to reduce major technical noises below fundamental ones, and the sensitivity is now limited by only known sources. Major technical noises have been identified and their projection is reconstructed through a model or a measured transfer function [1].

The next detector upgrade phase consists of the installation of new mirrors with Monolithic Suspensions. The new detector (here we name it *Virgo+MS* or *V+MS*) foresees a significant reduction of the thermal noise and increased sensitivity in the region below 100Hz (factor 3 to 7 with respect to Virgo+ design). Figure 1.2 compares the Virgo+ and Virgo+MS design curves [2, 3]. The sight range for NS-NS inspiral events will increase from 13Mpc (Virgo+) to 47Mpc [2, 3]. It is important to understand if technical noises are compliant with this challenge.
The fundamental noises of Virgo+MS (thermal noises, quantum, seismic, gravity gradient and residual gas), the new detector parameters and the new design curve are described in a separate document [3]. In this document we discuss all identified technical noises which are expected to contribute to Virgo+MS detector sensitivity. One Chapter is dedicated to each noise (Chapters 2 to 10). For each noise the current understanding of the noise is illustrated and a projection to the V+MS detector is presented and motivated. The noise reduction strategy, if necessary to comply with the design curve, is presented and its feasibility is discussed. Investigation studies and activities to pursue during the MS preparation phase are thus identified and described. Finally the full noise budget is compiled and discussed (Chapter 11).

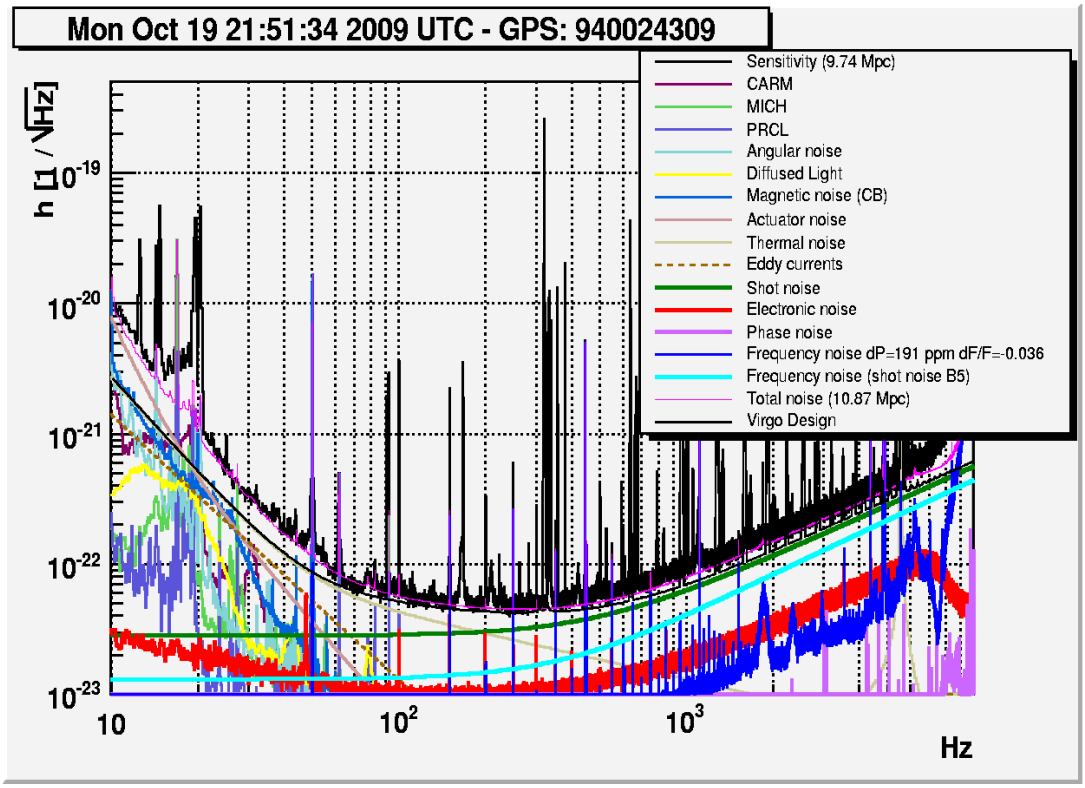

Figure 1.1*: Recent noise budget with input power P_0=17Watts and thermal compensation. The total noise (pink curve) also includes the expected thermal (pendulum and mirror) noises.*

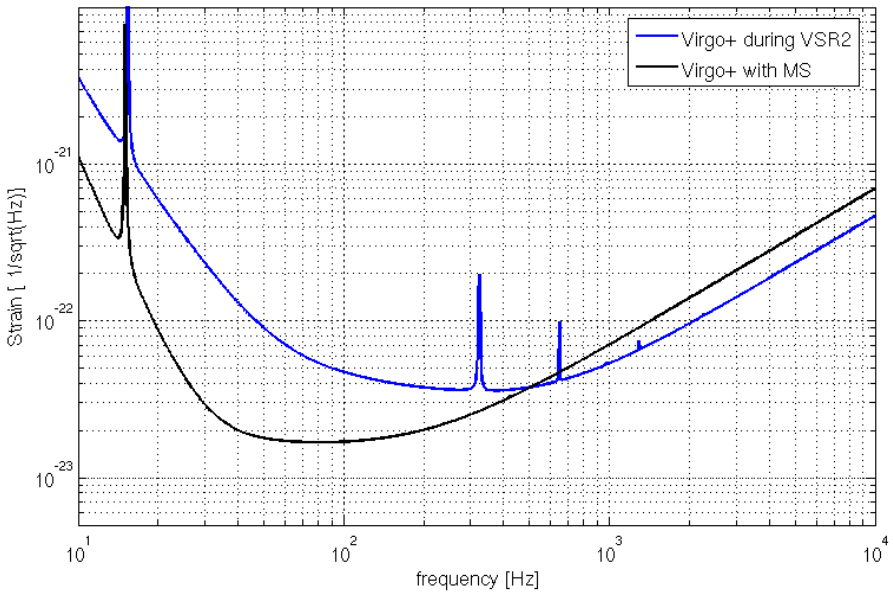

Figure 1.2: ***Virgo+ (blue) and Virgo+MS (black) design curves. The sight range computed for NS-NS of 1.4 solar masses with these curves is 13Mpc for Virgo+ and 47Mpc for Virgo+MS. This plot is taken from reference [3].***

2 Longitudinal control noise (G.Vajente)

A reasonable estimate of the longitudinal control noise contribution to V+MS noise can be obtained with the following assumptions:

- the same control scheme will be used for the locking of Virgo+ and Virgo+MS [4];
- presently longitudinal control noise is limited by photo-diode sensor noises which will remain the same for Virgo+MS. This is conservative, since noise hunting efforts should help in improving them;
- the same performances of noise subtraction (alpha, beta and gamma) will hold in Virgo+ and Virgo+MS.

Given these assumptions, we can consider the present measured noise projections for Virgo+ and reduce the MICH and PRCL contribution by a factor 3. This comes from the (simulated and measured) fact that the coupling of these two auxiliary degree of freedom residual motions scales with the arm cavity finesse. Figure 2.1 shows the detailed contribution and Figure 2.2 shows the total noise compared to Virgo and Virgo+MS design sensitivities.

It is clear from the figures that MICH and PRCL control noises will be compliant with V+MS design sensitivity, except for a few structures around 30-40 Hz, which are of environmental nature. Note that the structures around 20 Hz are calibration lines.
The main contribution to control noise will come from the CARM loop, which is presently locked on the reference cavity with 1.5Hz bandwidth. This error signal is quite noisy and if no improvement can be made it will be the dominant contribution and will strongly limit V+MS sensitivity.
However experiments are already being carried out to reduce this loop bandwidth down to 200mHz [5]. This new strategy seems feasible and it will completely remove CARM contribution to longitudinal control noise, at the level shown by the blue curve in Figure 2.2.

In conclusion, assuming the same level of sensor noise we have now in Virgo+, longitudinal control noise will give a contribution below the V+MS design sensitivity, assuming a better CARM control strategy, except around few structures of environmental origin.

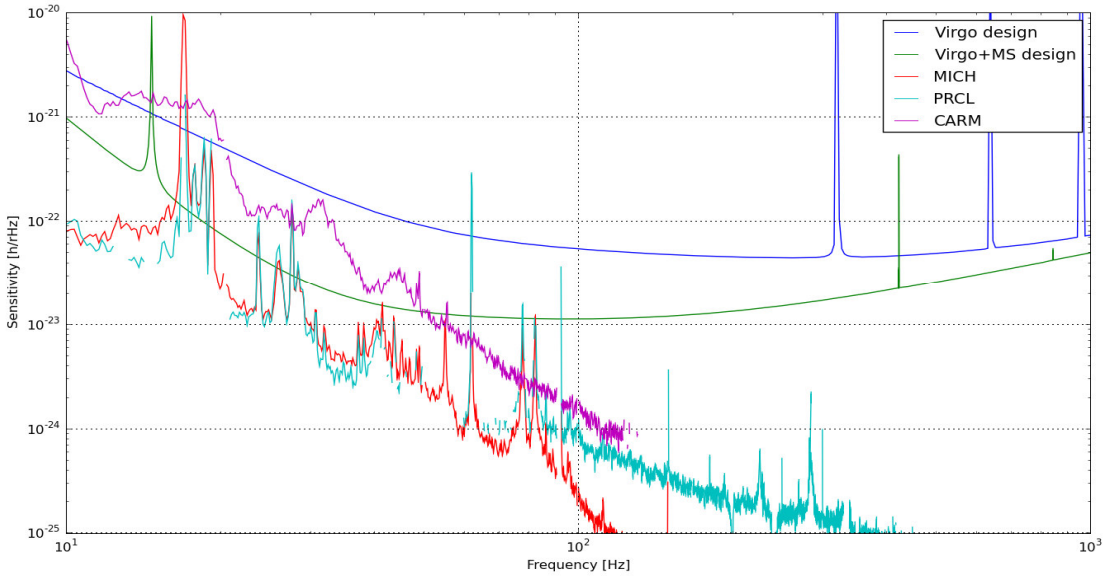

Figure 2.1: ***Projection of longitudinal control noise for Virgo+MS, individual contributions.***

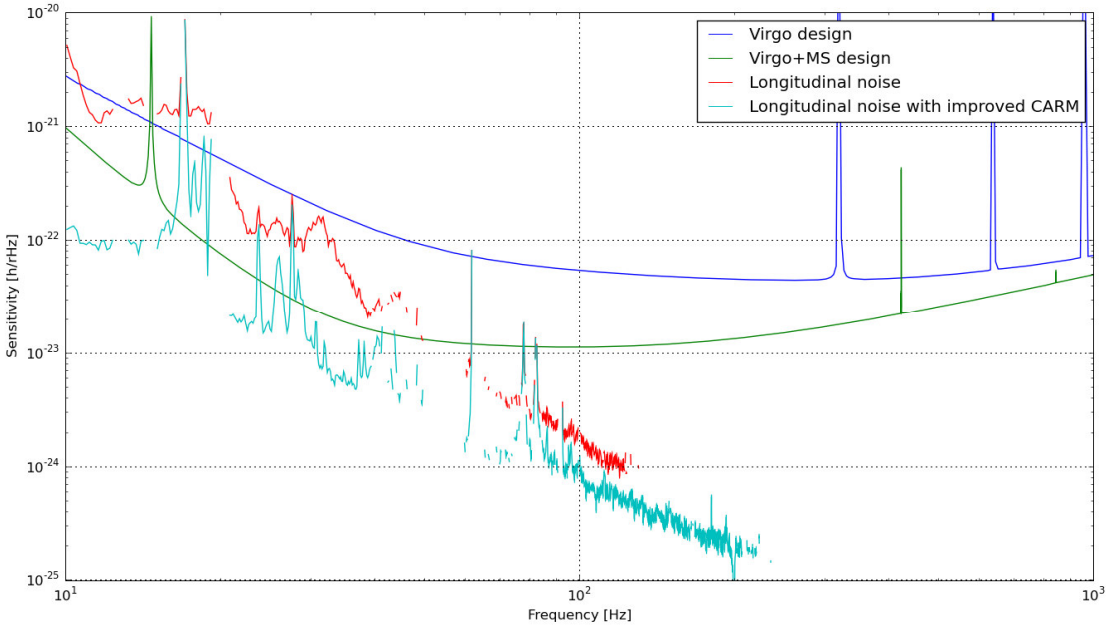

Figure 2.2: ***Total longitudinal control noise expected for Virgo+MS assuming the same control strategy or an improved one for CARM.***

3 Angular control noise (M. Mantovani)

In order to be able to evaluate the effect of the Automatic Alignment control noise in the V+MS configuration, considering also the monolithic suspension installation, the control chain has been simulated and the control noise has been projected to the V+MS design sensitivity.
The supposition taken into account in the following analysis, to be able to obtain realistic performances, is that the control chain for Virgo+MS will be improved only in the sensing part thanks to the installation of the new electronics and the optimization of the amount of impinging power on the quadrant diodes.
The propagation of the electronic/shot noise in the Automatic Alignment control loop chain is computed by using *Matlab* scripts, modeling the electronics, the control and the mechanics in the frequency domain, while for the transfer functions of the angular d.o.f. to the sensitivity the measured transfer functions have been considered.

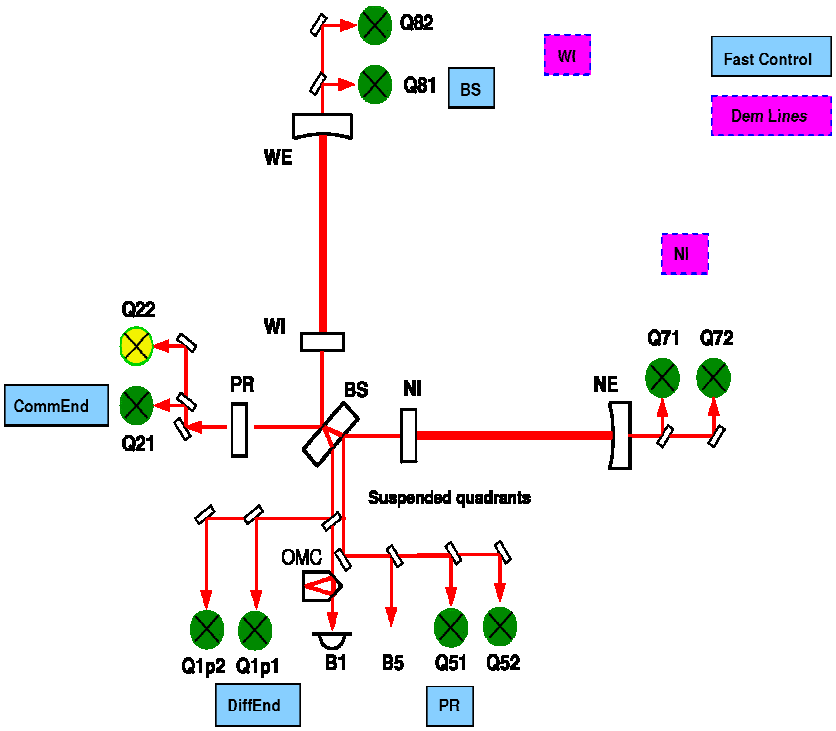

Figure 3.1: ***Initial Automatic Alignment control scheme for VSR2***

3.1 AA control scheme during VSR2

The angular control scheme during VSR2 is shown in Figure 3.1. The control is based on a mix of fast control, with a bandwidth of few Hz, for the Common Differential End, PR and BS modes and slow control, called Drift control with a bandwidth of some mHz for the input mirrors.
The Drift control consist in the modulation and demodulation of the input mirror angular displacement with frequencies below the detection band, from 7 to 9 Hz, to steer and center the beam on the terminal mirrors minimizing the longitudinal/angular coupling.

The most critical d.o.f. for noise performances are the ones which are controlled with the large bandwidth thus in the following only these degrees of freedom will be taken into account.
During VSR2 an improved control scheme has been implemented, which swaps the control of the *CommEnd* mode from the Q21 DC signal, which is strongly dominated by the EIB seismic motion at high frequency (above 10Hz) and by air current in the control bandwidth, to a combination of the suspended quadrants, on the suspended detection bench, DC signals.
The accuracy of the control has been improved by a factor ~3 and the error signal high frequency noise is lowered in the 10-20Hz region.
The current performance of the Automatic Alignment system fulfils the Virgo requirements for any frequencies in the detection band, as it is shown in Figure 3.2.

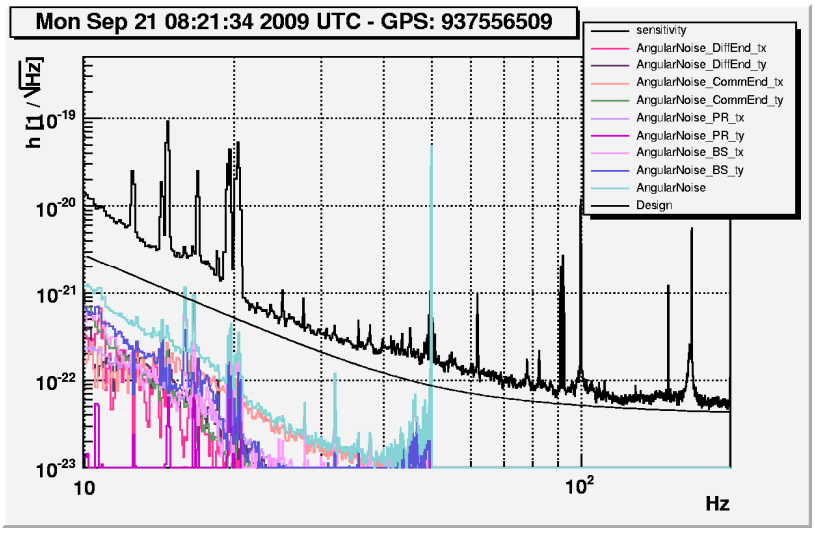

Figure 3.2: ***Automatic Alignment noise budget during VSR2.***

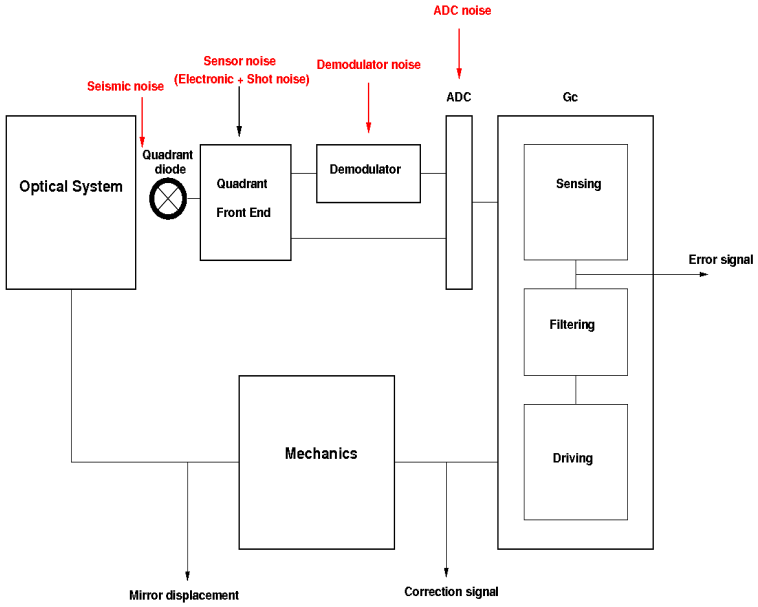

Figure 3.3: ***Automatic Alignment control chain, the noises are highlighted in red.***

3.2 Noise propagation

In order to evaluate the contribution of the Automatic Alignment control noise to the V+MS sensitivity the control chain has been modeled by using *Matlab* scripts, considering four different sources of noise:

- Environmental noise, seismic noise of the detection benches which affects the DC error signals (the measured seismic motion spectra have been used).
- Front-End noise, electronic-shot noise of the quadrant module.
- Demodulator board noise
- ADC noise

A scheme of the control noise simulation chain is shown Figure 3.3.
In order to have the best performance the power impinging on the diodes should be highest as possible, taking account the saturations in the sensing chain the gains of the electronics should be lowest as possible, in order to be limited only by shot noise.
The amount of power impinging on the diodes has been decided in agreement with the DET group. Moreover some margins of safety have been considered in the optimization in order to avoid saturations in the lock acquisition phase, since the RMS of the signals is much higher in this phase with respect to the science mode.

The optimized powers on the diodes are then:

Diode	Actual power [mW]	V+ optimized power [mW]
Q1p	0,0124	0,0160
Q21	0,0950	2,0000
Q51	1,68	5,0000
Q81	0,2700	16,5000

3.3 Limitations

The main limitation for the V+MS sensitivity achievement for the Automatic Alignment control noise is the ADC up-conversion.
The alignment signals have a very large dynamic, of about 10^6, which generates the up-conversion at the level of the ADC, thus the ADC noise which should be a flat noise of ~100nV/√Hz starts to rise as 1/f starting from ~100Hz.
This noise is actually limiting the Q21 and Q1p1 signals, which are used to control the Common and Differential End modes respectively, and it will increase as the error signal to noise ratio will increase since it depends on the signal dynamic.
The other limitation is due to the seismic noise which affects the DC error signals, which was limits the Common End error signal in the initial alignment configuration.

To control the Common End d.o.f. there are two possible control strategies. The first strategy consists in using the q21 DC error signal, the quadrant placed on the external injection bench used in the initial control configuration for VSR2, see Figure 3.4. The alternative is to use a combination of the quadrants placed on the suspended detection bench DC signals, see Figure 3.5.

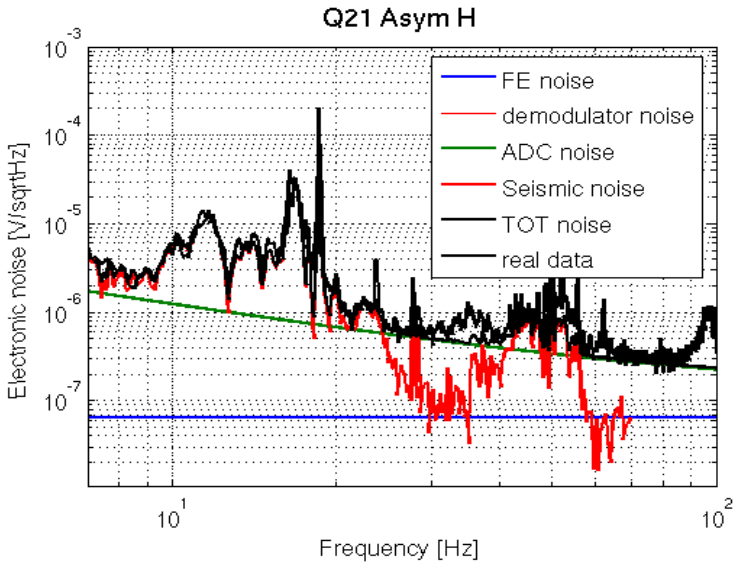

Figure 3.4: ***Q21 DC high frequency noise for the horizontal channel which is used to control the Common End tx d.o.f. in the initial VSR2 configuration for the AA control scheme. This signal is dominated by the EIB seismic noise, red curve, plus the ADC noise, green curve which is strongly affected by up-conversion.***

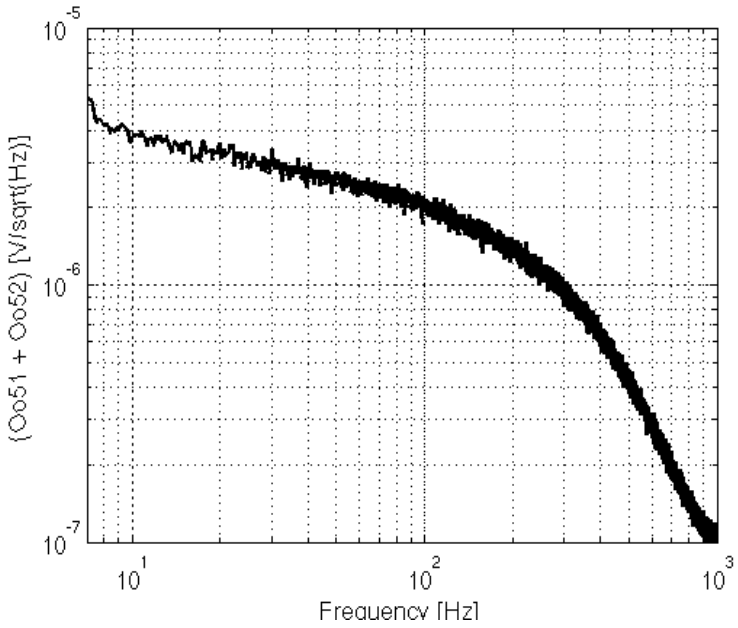

Figure 3.5: ***high frequency noise of the combination of the suspended quadrants DC signals used to control the Common End d.o.f. in the present configuration for the Automatic Alignment system, the shape of the signal suggests that also in this case the ADC up-conversion is present.***

The second configuration, the one which is presently running, has strong vantages such as the better low frequency accuracy, since the error signals are not affected by air current, and no seismic noise at high frequency, but still the error signal electronic/shot noise is too high for the V+MS requirements.

The idea is to maintain the control of the Common End d.o.f. at low frequency, up to some Hz, by using the suspended quadrants, to profit of the better accuracy and then use at high frequency, by mixing the signals if necessary, the most performing signal in term of noise.
In order to reach the design sensitivity for V+ the ADC up-conversion has to be solved, and if it will be solved only a factor of ~5 of improvement on the suspended quadrants noise can be reached.
While to improve the Q21 noise, apart from the ADC up-conversion reduction, the EIB has to be suspended.
The first option, using the suspended quadrants, will not be enough if a factor 10 of safety below the design sensitivity has to be considered since the Common End control noise will be 2e-22 at 10 Hz, while if the Q21 DC error signal will be used the signal to noise ratio can be improved by increasing the amount of light impinging on the diode.
For the environmental noise reduction on Q21 the suspension of the bench has already been planned while the ADC up-conversion is still under studies.

3.4 Radiation pressure effects

The major difference between the Virgo+ and the Virgo+MS configurations, apart from the better sensitivity, is the higher circulating power, of about 45kW. This could produce strong radiation pressure effects on the mechanical resonant frequencies of the cavity. As shown in Figure 3.6, the system remains stable and not critical.

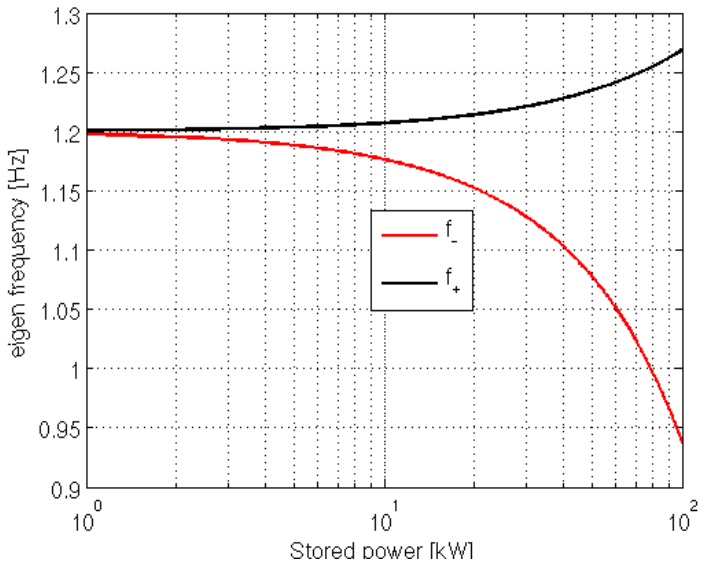

Figure 3.6: ***Radiation pressure effects on the resonant frequencies, the system remains stable.***

3.5 Noise propagation

The control noise has been then modeled and propagated in the control chain to the V+MS sensitivity. The analysis has been done considering that the seismic excess of noise on the Q21 DC signal and the ADC up-conversion has been solved.
As it is shown in Figure 3.7 and Figure 3.8, the simulated control noise is well below the design sensitivity of V+MS, in accord to the safety margin of a factor 10.
The only concern is that if the ADC up-conversion can not be solved, the behavior of the up-conversion has to be evaluated as a function of the dynamic of the signal in order to have a more realistic simulation.

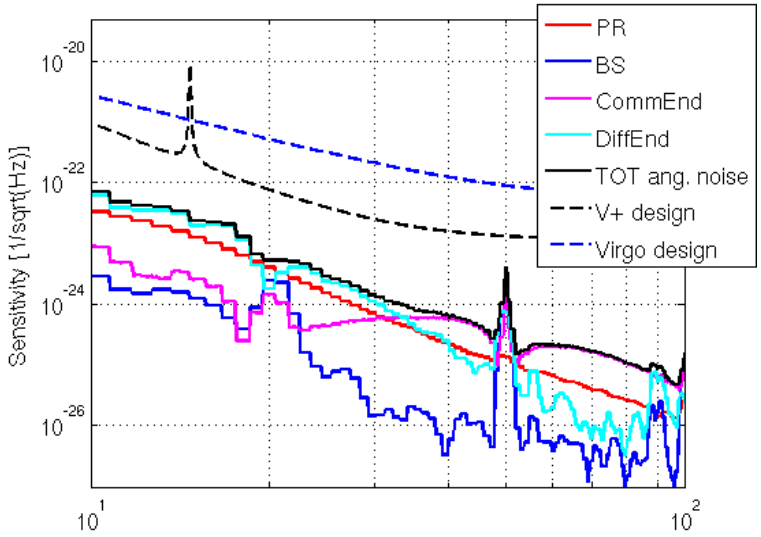

Figure 3.7: ***simulated control noise for the tx direction.***

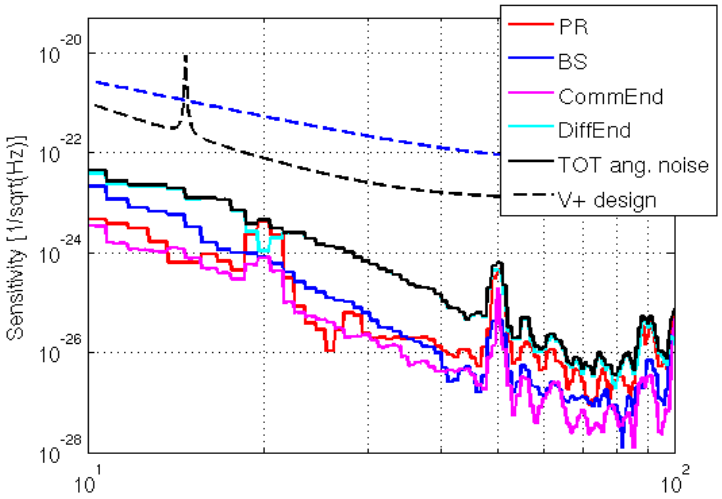

Figure 3.8: ***simulated control noise for the ty direction.***

4 TCS noise (V. Fafone, A. Rocchi)

The TCS installed in Virgo is based on a pre-stabilized CO_2 laser projector, that shines a heating pattern onto the HR surface of each input mirrors.
The TCS system can convert the intensity noise of the CO_2 laser into displacement noise through several mechanisms:

- Radiation pressure;
- Thermo-elastic: fluctuations in locally deposited heat cause fluctuations in local thermal expansion;
- Thermo-refractive: fluctuations in locally deposited heat cause fluctuations in local refractive index;
- Flexure: fluctuations in locally deposited heat cause fluctuations in *global* shape of the optic.

A detailed treatment of TCS noise couplings can be found in [6] and references therein. The overall expression for the strain is given by:

$$h_{TCS} = \frac{P}{2\pi f C \rho}\left(\Theta\left[(1+\sigma)\alpha\left(1-\frac{\pi}{2F}(n-1)\right) - \frac{\pi}{2F}\frac{dn}{dT}\right] - \frac{6\alpha}{h^2}C_{num}\right)\frac{RIN}{L} + \frac{P}{mc(2\pi f)^2}\frac{RIN}{L}$$

where P is the TCS power, Θ gives a measurement of the superposition between the IFO beam and the heating beam, RIN is the CO_2 laser relative intensity noise and C_{num} describes the coupling of the flexure noise. Besides the geometrical factors included in Θ and C_{num}, the noise introduced by the TCS depends on the power required for compensation and the CO_2 laser noise. In case of annular heating, the flexure noise is by far the dominant contribution.

4.1 Evaluation of thermal effects in V+MS

To have a quantitative estimate of thermal effects in V+MS, a precise knowledge of the new ITMs coating and substrate absorptions is necessary. As these measurements, at present, have not yet been performed on the new input mirrors, we considered confident values those measured at LMA on the Virgo ITMs: 1.25ppm for the coating [7, 8] and 0.7ppm/cm for the substrate [9, 10]. Even if recently [11] a value of 0.6ppm has been measured for the coating absorption, we considered 1.25ppm in order to be conservative. Thus, with a Finesse of 150, a recycling gain of 20 and an input power of 25W, the amount of thermal effects without TCS is expected to be around 2400ppm, in terms of coupling losses, defined as [12]:

$$L = 1 - |\gamma|^2 \text{ with } \gamma = 2\pi\int_0^a e^{ikZ(r)} |\Psi(\mathrm{r})|^2 \, rdr$$

where a is the radius of the test mass, $Z(r)$ the optical path length increase, k is the wave number and $\Psi(r)$ is the power density of the YAG beam. As a reference, the residual coupling losses, calculated for VSR2 with TCS on, amount to approximately 4000ppm.
The performances of the TCS have been simulated as a function of the annulus inner radius and CO_2 power, the outer radius has been kept at 14cm, equal to the present value. Results are shown in Figure 4.1.

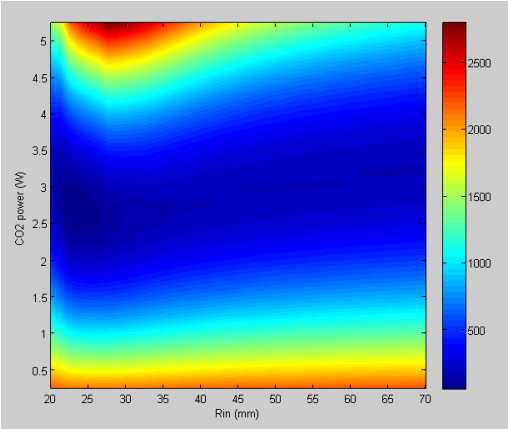

Figure 4.1: coupling losses as a function of the inner radius of the annular heating beam and of the CO_2 power

The minimum of the coupling losses is about 60ppm for 2.5W of power and R_{in}=25mm; this is the inner radius that has been used during the first tests on the TCS (the corresponding heating pattern is shown in the left image of Figure 4.2). Before starting VSR2, the inner radius has been increased to R_{in}=70mm (see right image in Figure 4.2). For this value there is a relative minimum of the coupling losses of 190ppm for 3.3W. We also considered a reduction of a factor of two of the thermal effects, i.e. 1000ppm residual coupling losses: for the two values of inner radius considered, approximately 1.0W and 1.3W of TCS power respectively are needed. TCS noise has been evaluated for these possible compensation levels.

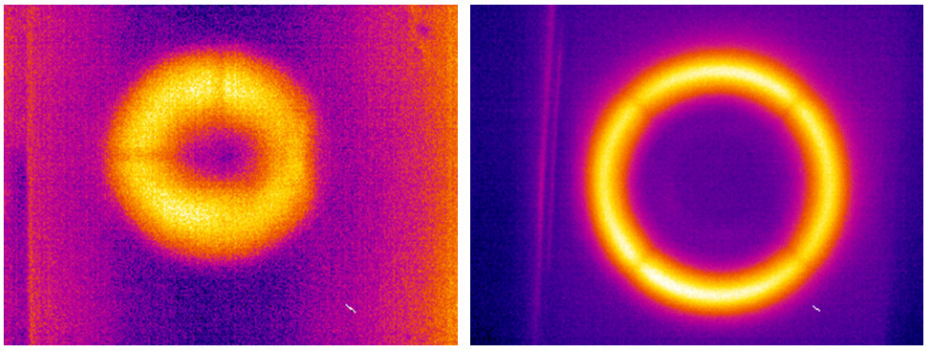

Figure 4.2: thermal images of heating patterns with R_{in}=25mm (left) and R_{in}=70mm (right)

4.2 TCS noise projections

The two values of the inner radius considered in the previous section have been used to calculate the corresponding values of Θ and C_{num}, reported in Table 4.1.

R_{in} (mm)	Θ	C_{num}
25	0.94	0.135
70	10^{-9}	0.074

Table 4.1: geometrical parameters used for the evaluation of the TCS noise

The other necessary parameter to compute the TCS contribution to V+MS sensitivity is the relative intensity noise of the CO_2 laser. At the beginning of October, after the studies carried on in Tor Vergata Laboratory [13], the intensity stabilization loop has been installed on the site (see Logbook entries # **25132** and **25196**). The closed and open loop noise spectra are shown in Figure 4.3.

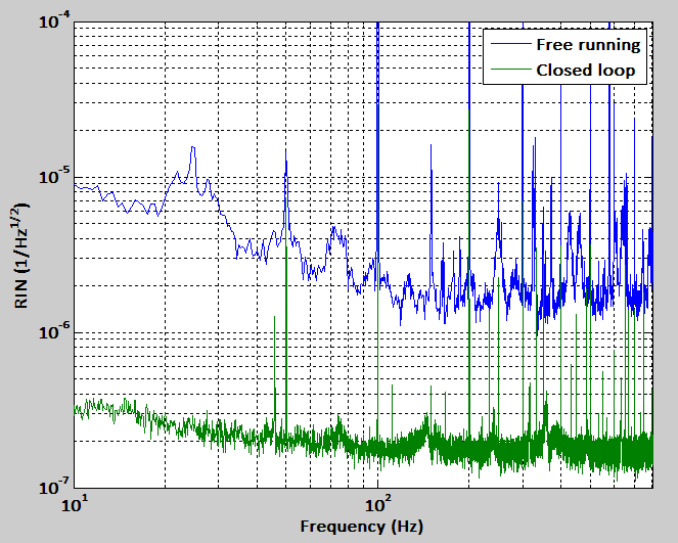

Figure 4.3: open loop (blue) and closed loop (green) CO_2 laser noise spectra

4.2.1 Compensation to 1000ppm residual coupling losses

In this case, as stated above, the TCS powers required are about 1.0W and 1.3W for a small and large hole respectively. Figure 4.4 shows the corresponding TCS noise projections, the blue and green curves refer to the CO_2 laser noise measured in Virgo, while the red curve represents the TCS noise evaluated for a flat *RIN*, averaging the floor of the laser noise spectrum.

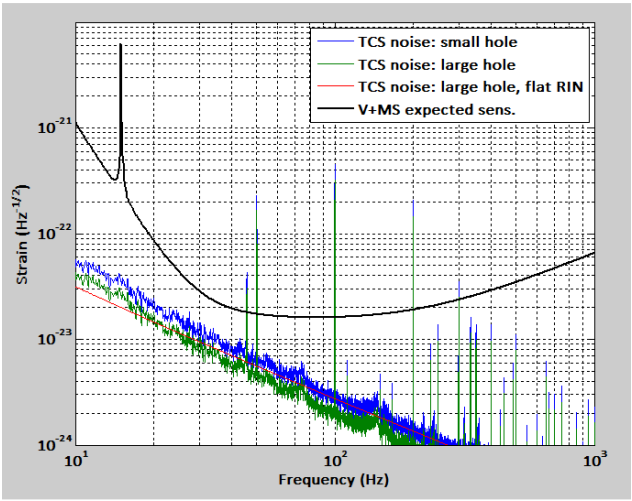

Figure 4.4: TCS noise projections compared to the V+MS expected sensitivity curve.

Looking at the graph above, we can conclude that in this configuration, the TCS noise is safely below the V+MS expected sensitivity at all frequencies.

4.2.2 Compensation to 60ppm-190ppm residual coupling losses

In this case, the TCS power required are 2.5W and 3.3W for R_{in}=25mm and R_{in}=70mm respectively. Figure 4.5 shows the corresponding TCS noise projections.

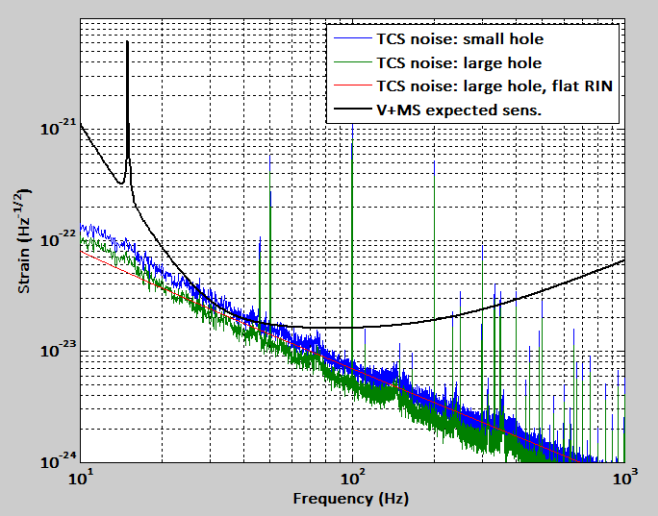

Figure 4.5: TCS noise projections compared to the V+MS expected sensitivity curve

For this compensation configuration, the TCS noise contribution to the V+MS expected sensitivity is not negligible. A reduction of the CO_2 laser noise of a factor of 3-4 is necessary. This could be accomplished by increasing the number of in-loop photodiodes to 9-16. In fact, the SNR scales as $\sqrt{N}$, where N is the number of photodiodes.

4.2.3 Coating absorptions two times higher than expected (2.5ppm)

The case of coating absorptions higher than expected has also been considered. In this scenario, coupling losses with no TCS would amount to 8000ppm. Again we studied both cases: reduction of coupling losses to the minimum values (optimal compensation) and reduction to half of the uncompensated value, i.e. 4000ppm (same as during VSR2). In case of optimal compensation, the required TCS power is 5.5W for inner radius of 25mm (residual losses of 230ppm) and 6.5W for an inner radius of 70mm (residual losses of 700ppm). Reducing coupling losses to 4000ppm decreases the power needed to compensate by more than a factor of two: 2.1W for R_{in}=25mm and 2.6W for R_{in}=70mm.

Optimal compensation in case of absorptions two times higher than expected is not feasible since a reduction of the CO_2 laser intensity noise of a factor of 10 would be necessary.

The case of VSR2-like compensation seems feasible (see Figure 4.6), provided a reduction of the CO_2 intensity noise of a factor of 3-4 is obtained by increasing the number of photodiodes to 9-16.

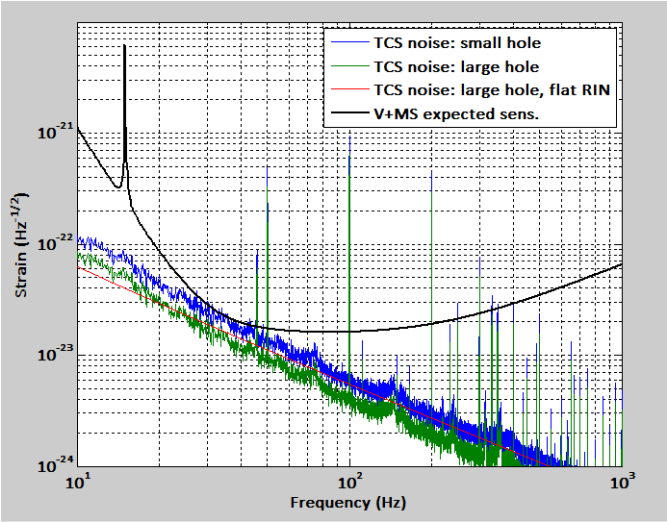

Figure 4.6: TCS noise projection for VSR2-like compensation with 2.5ppm coating absorptions

5 Diffused light (I. Fiori, E. Tournefier)

5.1 The mechanism of diffused light noise

Diffused light processes can couple seismic noise from the external environment into the interferometer. A fraction of beam power which impinges on vibrating surfaces (e.g. lens, beam dump, optical mount, optical window, vacuum tank inner walls) can be scattered back and recombine with the main beam. This type of noise is found relevant for frequencies below about 200 Hz, where the environmental seismic vibration is larger.
The noise produced in the gravitational wave signal by a generic diffused light source is [14]:

Eq.5.1 $$h_{bs}(t) = G\sin(\frac{4\pi}{\lambda}x(t))$$

where, $x(t)$ is the surface motion along the scattered beam direction, the quantity in parenthesis is the phase noise carried by the back scattered beam. The "coupling factor" G can be expressed as:

Eq.5.2 $$G = K\sqrt{f_{sc}}$$

where, f_{sc} is the fraction of light beam power impinging on the scattering object that is scattered back into the ITF opening angle, and K is a parameter that depends on the location of the scattering, and on ITF optical parameters.

As can be deduced from Eq.5.1, the coupling of diffused light is highly non linear in case of large displacements, typically for $\Delta x_{opt} > \lambda/4\pi$. Therefore if the scattering source is moving with a large amplitude (A_x) at low frequency ($f_x < 1$Hz) it can still spoil the Virgo sensitivity above 10Hz. If the amplitude of the displacement remains below $\lambda/4\pi$ harmonics of the main seismic peaks frequency show up in h, but for larger displacements an almost flat spectrum appears, up to a maximum frequency f_{max} with a rapid fall-off above f_{max} [14]:

Eq.5.3 $$f_{\max} = \frac{2A_x}{\lambda}2\pi\ f$$

5.2 Diffused light noise from external benches

External optical benches are significant sources of back scattered light. The case was well studied during Virgo commissioning and several mitigations have been performed [15]. For each external bench we have measured and estimated the value of G:

- we have measured G by shaking tests (for more details see Virgo Note [15]);
- we have estimated G values, based on measured back scattering properties of optic elements on the external beam path (to estimate f_{sc}), and based on ITF optical parameters. This is described in one Virgo note [14].

Table 5.1 lists measured and estimated G values for external benches. The good agreement indicates we have reasonably good understanding of diffused light from these benches. This permits to do reliable extrapolations to Virgo+MS, accounting for its different optical parameters.